Forschung im Ingenieurwesen (2025)89:9
https://doi.org/10.1007/s10010-025-00785-3

ORIGINALARBEITEN/ORIGINALS

Quasi-static modeling of long-wave axis deviations in planetary gears for transmission error signal analysis

Simon Nohl[1] · **Christian Westphal**[1] · **Christian Brecher**[1]

Received: 20 September 2024 / Accepted: 29 January 2025

Abstract
Planetary gears are widely used in large transmission applications, such as wind turbines, hydropower plants and industry, due to power density, high gear ratio and efficiency advantages. The advancement of predictive maintenance and gear system design processes is essential to enhance the ratio between durability and used material of gearbox components. Preventing possible downtime due to unforeseen failures in between maintenance intervals also increases resource efficiency. In this paper, a quasi-static FE-based method is presented that calculates the running behavior of planetary gear stages considering time variant and time invariant axis misalignments, tooth flank deviations as well as the influence of coupled meshing areas. A contact algorithm is presented, taking into account load dependent deviations of an adjustable sun gear onto the contact behavior, which is widely used to compensate load-sharing issues. The model can consider these deviations and their influence on the contact behavior hence their characteristic frequency order spectrum. In the future, vibration signatures taking into account manufacturing as well as load dependent deviations can be created to help identifying misalignments in transmission error data. The method can then be used for end of line tests as well as the evaluation of the rest of useful life based on local pressure distributions and tooth root stresses.

Abbildung langwelliger Achslageabweichungen in Planetengetrieben zur Signalanalyse des Drehwegfehlers in der Quasistatik

Zusammenfassung
Planetengetriebe werden aufgrund ihrer Leistungsdichte, ihres hohen Übersetzungsverhältnisses und ihrer Effizienzvorteile häufig in großen Getriebeanwendungen wie Windkraftanlagen, Wasserkraftwerken und in der Industrie eingesetzt. Die Weiterentwicklung der Zustandsdiagnose sowie der Auslegung von Getrieben ist unerlässlich, um das Verhältnis zwischen Lebensdauer und verwendetem Material von Getriebekomponenten zu verbessern. Die Vermeidung von Stillstandzeiten aufgrund unvorhergesehener Ausfälle durch die Zustandsdiagnose zwischen Wartungsintervallen erhöht ebenfalls Ressourceneffizienz. In diesem Artikel wird eine quasi-statische FE-basierte Methode vorgestellt, die das Einsatzverhalten von Planetengetriebestufen unter Berücksichtigung zeitvarianter und zeitinvarianter Achsabweichungen sowie Flankenabweichungen abbildet. Es wird ein Kontaktalgorithmus vorgestellt, der zusätzlich ein einstellbewegliches Sonnenrad berücksichtigt, welches häufig zur Kompensation von Lastaufteilungsstörungen eingesetzt wird. Das Modell kann diese Abweichungen und ihren Einfluss auf das Kontaktverhalten und damit auf ihr charakteristisches Frequenzordnungsspektrum berücksichtigen. In Zukunft können Schwingungssignaturen erstellt werden, die sowohl fertigungs- als auch lastabhängige Abweichungen berücksichtigen und die Information der Verlagerungen für End of Line Tests sowie Algorithmen der Zustandsdiagnose verwendet werden.

1 Introduction

In addition to increasing power density, predictive maintenance processes for wind turbine gearboxes and other large gearboxes must be advanced, in order to also enhance the ratio between durability and used material. Studies on the

✉ Simon Nohl
s.nohl@wzl.rwth-aachen.de

[1] WZL, RWTH Aachen University, Campus-Boulevard 30, 52074 Aachen, Germany

Published online: 10 February 2025

causes of downtime and the effect on energy costs show that over the service life of a wind turbine, gearbox failures lead to the longest downtime in onshore as well as offshore applications [1]. Further, the in the field appearing load collective, which was considered to be a nominal load collective in the design stage, varies and thus affects the lifetime of wind power gearboxes possibly leading to early failure [2]. Additionally, over the circumference varying flank deviations, planet axis misalignments and all planet carrier, sun and ring gear misalignments are known to have an effect on tooth to tooth differing load distribution as well as low frequency and sideband excitation in wind turbine gearboxes [3]. Deviations with such effect are characterized as long-wave deviations.

In the wind power sector, condition monitoring systems have been used for a long time to monitor the health of gearbox and system components as well as estimating maintenance intervals [4]. Vibroacoustic condition diagnosis as part of condition monitoring systems includes the recording and interpretation of the excitation signal of cyclostationary moving machine elements [5]. In gearboxes based on the gear mesh frequencies and rotational frequencies of the shafts, especially sidebands in the excitation frequency or order spectrum can be used to identify and classify fault mechanisms [6]. Based on a trend interpreter, the need of maintenance can be triggered and permitted loads decreased to prevent damage of the superordinate system.

Planetary gearboxes live up to today's standards of high power density and transmission ratio with high efficiency. Specific behavior of planetary gearboxes is resulted mainly due to the coupled out of phase planetary meshes as well as the high number of possibly deviated elements and their kinematic and kinetic relationships. In addition, planetary gearboxes are more deformable during manufacturing as well as operation due to the reduced use of material for the same transmission power, which also has an effect on the long-wave excitation behavior [7].

Various calculation methods are being developed and investigated to consider the contact behavior of planetary gears. The Finite-Element-based (FE) simulation is particularly useful to optimize the running behavior of planetary gears in the design stage. However, the influence of misalignments on the contact ratios and contact line positions in planetary gears as well as the influence of long-wave deviations on the operating behavior cannot be taken into account in existing non-commercial approaches. Therefore, the FE-based tooth contact analysis as presented in this paper was extended, in order to investigate the system influences on the contact behavior of planetary gears as well as the transmission error (TE) and its frequency spectrum. Focus lies on considering and analyzing the long-wave excitation behavior. Based on the findings, new methods for the design on the one hand and a characterization of deviations on the excitation spectrum for more accurate rest of useful life prediction models on the other hand can be provided.

2 Simulation models of planetary gears

Simulation models for planetary gears essentially comprise the following methodical approaches. Phenomenological models are based on periodic modeling of characteristic excitation frequencies of planetary gears to consider modulation effects and excitations for vibration diagnostics and frequency order tracking. A known model was developed by Inalpolat and Kahraman, a more recent model for double helical planetary gear sets was developed by Götz [8, 9]. Advantages are fast computing time and information regarding excited frequencies also for stationary acceleration sensors. However, load-related effects and displacements can only be considered analytically, time-variant transfer paths described as Hanning functions and acceleration amplitudes must be normalized with experiments.

Especially for high-speed applications, dynamic models have a high information quality with the disadvantage of increased calculation times. For each time step, a lumped parameter model described by mass inertia, modal stiffness and damping models is solved in the form of differential equations. The coupled meshing areas in planetary gears increase the computational effort even further. In current research of vibroacoustic diagnostics dynamic models are mostly used due to the implied consideration of the transfer paths to the gear housing depending on the modeling depth. In the rigid-flexible coupling model of a planetary gear system developed by Zhang et al. a signal extraction position on the housing was used to receive sensor equivalent data of the system vibration response [10]. Hanning functions for transfer path modeling is also used, for example in the models from Feng and Zuo as well as Inalpolat and Kahraman [11, 12]. The meshing stiffness in dynamic simulation is modeled by bending beam elements or a qasi-statically precalculated mesh stiffness; an approach on modeling dynamic meshing stiffness was developed by Xie and Yu [13]. Westphal et al. developed a dynamic model for stepped planetary gear stages taking into consideration meshing stiffnesses and tooth flank topographies modeled by a line contact approach in the meshing areas [14]. The influence of gear faults like tooth root cracks, pitting, spalling and other defects on the meshing stiffness is also being investigated, whereby the faults and their meshing stiffness influences are described analytically [15–17].

Quasi-static calculation models neglect mass inertia and general damping effects. They can be divided into methods that calculate the tooth contact problem with a direct FE-solver and methods with a spring equation system solver.

The contact stiffnesses in spring equation system methods is either calculated analytically or with a direct FE-Solver. The Latter are considered as FE-based quasi-static methods. These models separate the stiffness calculation of gear structures using an FE solver from a subsequent tooth contact analysis using a linear equation solver. This enables the stiffness calculation to be carried out independently of the solution to the contact problem leading to reduced calculation time compared to direct FE-solving methods.

Softwares that feature direct FE-solving algorithms specifically for gear design are Marc© as well as Ansys©. Commercial software systems with an FE-based approach and predetermined contact lines are widely used such as in deviations and flank topographies are considered indirectly by additional contact distances in the meshing area. Examples are Vibragear©, Romax©, Masta© and Genom©. These Simulation softwares show significantly reduced calculation time, as analyzed by Bejar. While the direct FE-solving methods imply out-of-action contact lines, Romax© and Masta© feature a model approach to consider extended load dependent line of action in addition to the predetermined contact lines. Bejar states that the results concerning corner contact differ between all program systems [18].

Stirak, an FE-based tooth contact analysis extended by Schäfer, determines contact stiffnesses and the influence of gear body structures in relation to FE-nodes of the involute tooth flank areas [19]. This is achieved by applying unit forces on the center of the tooth flank surfaces of the underlying elements according to analytically precalculated contact lines depending on the ideal contact geometry. The deformation information is then saved as displacement influence coefficients (DIC) for each contact line for each discrete rolling position. The underlying assumption for further proceeding is that the superimposition of single deformations by unit loads is scalable depending on the normal force and thus the torque due to linear elastic material behavior. The normal force is made up by the sum of the nodal forces but the force distribution is unknown and is defined as the contact problem. In the tooth contact analysis, the tooth flanks are rolled incrementally and tooth flank deviations in the meshing area are considered by contact distances deviating from the ideal involute. The contact problem is transferred into a spring model with all potential contact points on the contact line described by the contact distance and their DIC in a linear system of equations which is solved until all contact pairs with negative contact forces are eliminated [20]. This method has been continuously extended for planetary gear simulation [21–23]. Due to the contact algorithm, axis misalignments are converted into additional contact distances while the contact line position itself remains unchanged [24].

Ahmad extended the program system of the previously described tooth contact analysis for cylindrical gears by the consideration of long-wave axis misalignments as well as pitch deviations and investigated the influence on the excitation behavior of electric vehicle gearboxes [25]. These deviations are calculated into flank topography data, which are then calculated to additional contact distances onto the contact lines. After experimental validation, Ahmad used the method to derive analytical functional parameters for an excitation-oriented tolerancing of long-wave deviations [25].

The findings of the previously described work as well as the extension of the program system cannot be directly transferred to planetary gears due to the coupled meshing areas and general operating conditions that require the modeling of contact line shifting under load. For cylindrical gear stages, the tooth contact analysis Zako3D was developed by Hemmelmann, in which the tooth contact is modeled with a numerical surface contact instead of analytical line contact being able to consider premature tooth meshing and contact line shifting [26]. The method is able to consider long-wave deviations within the calculation procedure but the kinetic and kinematic behavior of planetary gears is not modeled.

Quasi-static calculation models are mainly used in gear design applications. The calculation of tooth root stress, flank pressure, excitation behavior based on the static transmission error (STE) and efficiency is performed in short calculation time especially with methods that solve the tooth contact with spring equation systems. According to the current state of the art, phenomenological models offer a faster calculation approach for characteristic excitation frequencies for condition diagnosis algorithms. Dynamic models can provide information about the transfer path as well as additional dynamic load effects. In addition to signal analysis, the focus in dynamic modelling is also on fault seeding and the influence of tooth damage on the contact stiffness and consequently on the measured acceleration signal of a sensor. Correlating the excitation behavior and other operating data with manufacturing- as well as load-related displacements could be an alternative approach to make a failure prediction based calculating the time varying local resilience. Collecting the historical resilience data and accumulate it to a load collective could predict the end of useful life much earlier. Quasi-static methods would be advantageous for this due to calculation efficiency. Manufacturing- and load-dependent deviations, especially long-wave deviations, and their influence on the running behavior are mainly considered in commercial FE-based methods for planetary gears. These software solutions calculate axis deviations onto the load-free and analytically predetermined contact lines onto the flank topography and use model approaches for out-of-line contacts under load. The

consideration of deviations in the contact areas directly is not possible due to the contact algorithm approach. Also, in these methods it is not apparent, if the deviations calculated onto the flank topography vary with every discrete rolling step, every base pitch or whether a change of the magnitude of the deviations with a fluctuation of the working operating pressure angle α_{wt} is considered. Further, with an increase in flexibility of the gear system, due to weight reduction of the gear wheel bodies, shafts and housing as well as the usage of adjustable elements for better a load distribution in planetary gear stages, a contact approach that solves the tooth contact under cross influence of surrounding elements is needed.

3 Objective and approach

To analyze the effect of long-wave deviations on the running behavior of planetary gears, the objective is a quasi-static tooth contact analysis considering displaced meshing conditions including time varying axis misalignments. For this purpose, a new contact algorithm was developed considering the load-dependent and kinematic conditions of a planetary stage, taking into account displacements during a complete roll-over in quasi-statics. The approach for achieving the objective is shown in Fig. 1. The initial method carrier was developed by Westphal et al. for calculating cylindrical gear stages in dynamic simulations with a surface contact algorithm based on Hemmelmann and the spring model routine based on Neupert [20, 26, 27].

In step 1, the contact model is extended for a planetary gear stage with coupled meshing areas. For this, a specification of deviations of the gear and planet-carrier (PC) axes is to be implemented. As the existing method calculates a single mesh using the influence coefficient method, a system of equations is to be set up and solved by combining the displacement influence coefficient matrices and considering kinematic and kinetic boundary conditions for planetary gears. In the industry, adjustable elements are used to compensate unequal load-sharing [28]. For this reason, an algorithm is to be implemented to consider the behavior of a flexible connection on the sun shaft. In addition to the surface contact approach for higher computational efficiency of the linear equation solver of the coupled spring model, a numerical line contact approach is transferred to the planetary gear stage contact model.

In step 2, the method is verified by comparing meshing sequence variants and their load distribution as well as STE variation. The verification is based on a comparison with a validated FE-based method by Theling, who extended the FE-based tooth contact analysis Stirak presented by Schäfer, in which planetary gears are modeled using an analytical line contact approach [19, 23].

In step 3, the influence of long-wave deviations on the excitation behavior of a planetary stage with sequential and symmetrical meshing sequence without and with adjustable sun is simulated. A single eccentricity and a wobble deviation of the planetary gear is considered. Finally, the modulation effect due to an axis misalignment of a fixed ring gear is investigated and the functionality of the method is verified.

4 Simulation method for deviated meshing areas in planetary gears

This chapter presents the simulation method developed for calculating the operational behavior of misaligned planetary gear stages. The calculation method is illustrated in Fig. 2. Geometry and operating data are specified as input variables for the calculation method. In addition, axis misalignments as well as eccentricity errors and wobble deviations with their respective phase angle can be specified. Further, an interface was created to specify individual tooth deviations and pitch errors, concentricity errors and shaft position deviations from measurement data.

Based on the specification of the macro geometry firstly, node mesh coordinate data files are generated which are then converted into FE-structures in Nastran format. The next step is to calculate the DIC of the FE-structures on

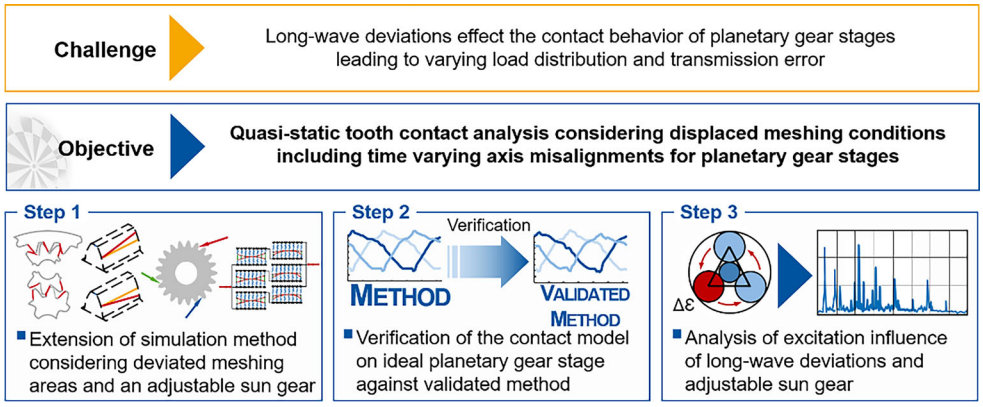

Fig. 1 Objective and approach

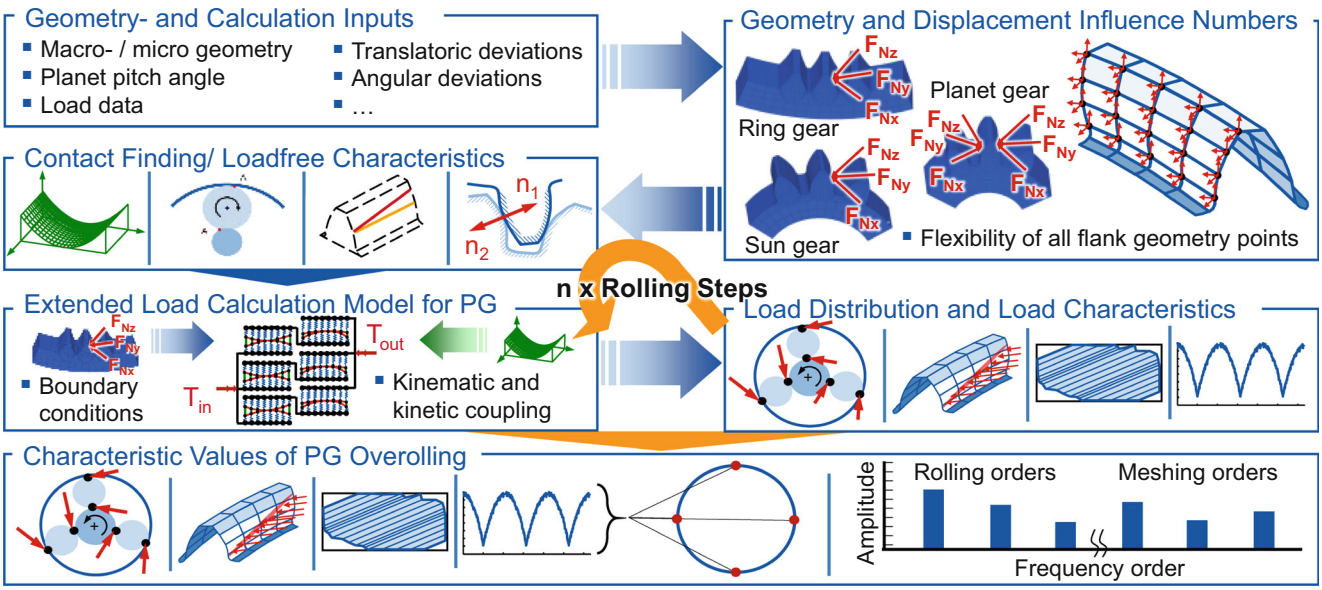

Fig. 2 Calculation procedure of the simulation model of planetary gear

the tooth flanks independently of the contact line for each flank element. Compared to Stirak, it offers the advantage of an independent determination of contact areas [19]. For one macro geometry, the DIC calculation has to be carried out only once for each gear wheel. This means that a new FE-calculation does not have to be carried out for a new specification of flank topography or axis misalignment.

After calculating the displacemenet influence coefficients, the tooth contact analysis is performed for the input data set. Initially, the system is brought into contact and the tooth flanks are rotated in discrete steps according to the operating configuration. Based on the initial contact determination, the specified displacements are applied and the system is rotated until there is no penetration of the contact flanks. In this way, the load-free STE on the one hand and the contact distances of each contact field on the other are determined. In the next step, the spring model for the load calculation is set up and solved for the rolling position using the load-free contact distances and the DIC. It is interpolated to the contact point pairs in the normal direction of the drive wheel depending on the power flow. The system of equations corresponds to the system of equations set up by Heider, which is also used in the validated method [23, 29]. The load distribution between the planets as well as on the tooth flanks results from the solution of the linear system of equations. The load-dependent STE is evaluated based on the rigid body rotation, which must be the same for all central gear meshing areas. The calculation steps described above are now repeated until all rolling positions have been calculated. Time-variant misalignments, analytically as well as from measurement data, are also resolved via the rolling increment and taken into account in the load-free contact algorithm. The deviations applied by consecutive tooth numbering of teeth in contact. Once the calculation of each rolling position has been completed, the flank pressures and tooth root stresses are calculated for base pitch and a transformation of the STE to the frequency order spectrum is performed related to the PC rotation.

The steps for the initial contact algorithm are shown in Fig. 3 using two planets with power flow from sun to ring gear. The meshing areas are currently considered as separate models and aligned with each other according to the geometric boundary conditions. The aim of the penetration-based contact determination is to determine the rotation angles of the gears for the STE calculation on one hand and the contact distances for the spring model on the other. First, the reference gear pair is aligned, which is located at the 12 o'clock position. This is achieved by performing rotational operations on the node mesh coordinate data files of the tooth flanks. The middle flanks of the sun and planet are rotated until the minimal contact distance between the flank points converges towards zero. The contact distance calculation is a core component of the underlying method for single gear pair meshes and has been adopted for this method, see Fig. 3 right [27]. Since the nodal grid points in rotational direction φ is congruent only in aligned case with same gear face width, the grid points of the output tooth flank are interpolated in order to be congruent to the flank points of the input tooth flank, which is set as reference flank according to the power flow. To calculate the minimum contact distance, the point on the reference flank with the smallest rotation angle distance between the flanks is determined from all possible contact points. Furthermore, the penetration point in the direction of the reference flank

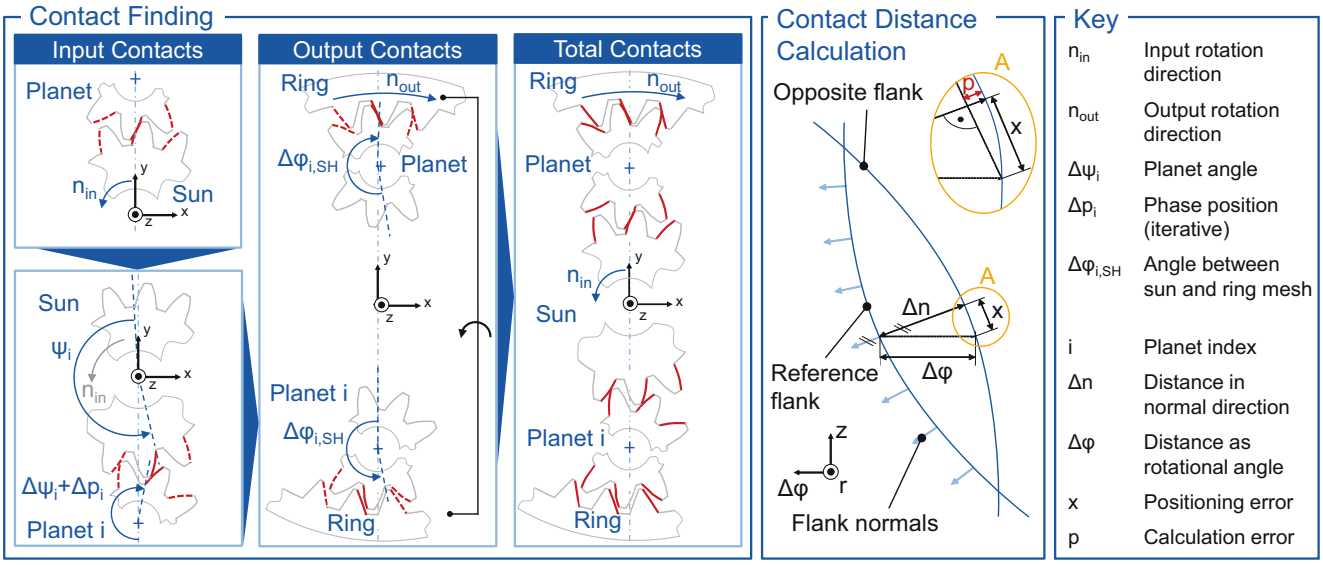

Fig. 3 Contact finding and calculation of contact distances

normals Δn, which are assumed to remain common also under load, is determined using orthogonal projection [27].

Once the reference gear pair has been defined, the other meshes are positioned in relation to the reference mesh according to the transverse normal base pitch closest to the given planet position angle Ψ, see Fig. 3 bottom left. In this case, only the planet flanks are rotated since the angular position of the input gear is already determined. Next, the meshes on the ring gear are prepositioned using the planet flanks as a reference analog to the step before. Now, the flank points only of the output gear, in this case the ring gear, are iteratively rotated together until there is no penetration at any of the contacts. As the system is already staticall y overdetermined if there is more than one planet, there will be gaps at the other meshing points. Result are now the rotation angles of all tooth flanks of all gears for all rolling positions, since the incremental rolling position step is linear and the distance between other tooth flanks on one gear, is defined by adding or subtracting the transverse normal base pitch angle. After the ideal positioning was exercised, all other deviations are taken into account and the algorithm starts by repositioning the planets on the input meshes and the output gear flanks on the output meshes afterwards. After determining the position angles in the final position for each rolling position, the final calculation of all contact distances in all meshing areas is performed and handed over to the load calculation. While the DIC of the nodes can be adopted for the reference flank as for the contact distance calculation, the DIC for the mating gear must be interpolated through the penetration point in the normal direction of the reference flank. This is done directly via the conversion according to the shape functions of the linear hexahedrons used; a quadratic compensation polynomial is not used. Linear hexaedrons are used analogous to the tooth contact analysis Zako3D developed by Hemmelmann, because the determination of contact line independent DIC for all flank surface nodes takes significantly more time than the use of contact line dependent DIC used in Stirak [26]. Additionally, to achieve comparable STE curves and converged flank pressure values, a higher number of tooth flank nodes have to be set. For Zako3D the number of profile and lead direction nodes of pxl = 61 × 61 have shown good convergence as determined by Willecke to predict STE values based on flank topography data with a surrogate model compared to the tooth contact analysis simulation data [30]. These values are used for all following simulations and compared to Stirak simulation results with half the number of elements due to use of quadratic elements in the analytical line approach, see Chap. 5.

With the new contact algorithm extended for planetary gears, an iterative routine was developed in order to take into account a reduced shaft connection stiffness of the sun gear. In the approach, a uniaxial bending stiffness K and the distance of the connection to the sun gear center are specified for a rigid sun shaft. After the first calculation of the load distribution between the planets of one rolling position, the operating pressure angles of each planet-sun-contact are determined on the basis of the center distances and the base circle diameter of planet and sun gear [31]. The partial radial forces of each planet i in the x and y directions of the global coordinate system are calculated depending on the operating pressure angle $\alpha_{wt,i}$ and the planet position ψ_i, whereby the reference position $\psi_i = 0°$ corresponds to the planet position in the 12 o'clock position. The radial forces are then superimposed and the sun

Table 1 Gear data

Meshing sequence variant	Symmetrical [33]	Asymmetrical [33]	Sequential
Number of teeth z sun/planet/ring [–]	15/16/–48	14/16/–46	22/17/–56
Center distance a [mm]	105	101.373	112.5
Normal module m_n [mm]	6.5	6.5	5.2
Pressure angle α_n [°]	20	20	20
Helix angle β [°]	0	0	21.5
Gear face width b [mm]	70	70	45
Number of planets *n* [–]	3	3	3
Planet position angle $\Psi_{2\text{-}1}/\Psi_{3\text{-}2}$ [°]	120/120	114/114	120/120

gear is radially moved according to the resultant forces and the specified connection stiffness and tilted according to the connection distance. The radial displacement of the sun gear tooth flanks are now again misaligned in the different meshing areas of the different planets. The load-free contact alignment is then carried out again, so that there is no penetration between the tooth contacts and the additional displacement of the sun is taken into account in the load-free STE. In the next step the spring equation system is set up again and solved under load. The procedure is carried out until the amount of displacement of the sun falls below a limit value of $\Delta s = 1\,\mu m$ which means that the sun displacement is in quasi-static equilibrium to the resultant of the radial forces multiplied by the radial compliance. At the end of a complete contact simulation, the method outputs the x- and y-coordinates of the sun orbit over the discrete rolling steps.

Due to the requirement of solving the spring model several times to determine the sun displacement, solving full surface areas in the spring model takes too much computational effort. Therefore, a numerical line contact according to Westphal et al. was applied to the model; the contact distances in each meshing area are reduced equidistantly to one possible contact point per profile line by fitting a quadratic polynomial on the reference flank [32]. Each tooth has one interpolated line of discrete springs over a possible line of action brought into the spring model, so that also premature tooth meshing under load can take place. Additional profile line points getting into contact under load are no longer taken into account. The contact line shifting due to displacements is still considered due to the developed contact finding algorithm.

5 Verification of the simulation method

The method was verified using two planetary stages with different meshing sequences from Papies' work, see Table 1; [33]. Since the total contact ratio ε_γ of all meshes of both spur gear variants is between one and two, the phase position can be verified using the teeth in contact. The validated method, which is used to verify the correct simulation of the meshing phase, load distribution and STE of the newly developed method, is based on Stirak with an analytical line algorithm and was developed by Theling for planetary gear stages [23]. The meshing sequence on the planet from sun to ring gear in this method are analytically determined using the calculation method developed by Piel in order to align the rolling paths of the meshing areas considering the planet positions and tooth thickness [34]. The results of the planetary stage with symmetrical meshing sequence are shown in Fig. 4.

The variant has an in-phase or meshing sequence of all planets at the sun gear at the discrete rolling position $i_{RP} = 30$ as three teeth come into contact simultaneously, which corresponds to the analytically calculated meshing sequence, see Fig. 4 top. The total number of meshing teeth of the planetary stage is compared load-free and under load with the validated method. Without load, the number of teeth in contact between the developed method and the validated method matches with deviations of a maximum of one rolling position. Under load, there is no premature and late tooth meshing with the validated mehod due to the analytically calculated contact lines. The new method shows both effects under load. The load distribution between the planets is ideal for both methods, see Fig. 4 centered.

The STE-varation from sun to ring gear shows very good correlation between the methods, see Fig. 4 bottom. Due to the load-related increase in contact ratio, a smaller fluctuation in TE occurs with the new method. The premature tooth meshes at rolling position $i_{RP} = 27$ for the sun and $i_{RP} = 13$ for the ring gear leads to an increase in the STE compared to the validated method. The peak-to-peak Fast Fourier Transformation (FFT) also shows very good correlation between the methods up to the higher harmonics of the tooth mesh order. The first and second tooth mesh orders O_m in particular are excited, as on the one hand all meshing on a central gear takes place simultaneously and on the other hand all tooth meshes on the ring gear take place about half a base pitch earlier.

The verification results of the asymmetrical variant are shown in Fig. 5. Starting from the reference planet at 12 o'clock, the planet position angles ψ of the planets are $\Psi = 114°$ each. The load-free phase positions of the

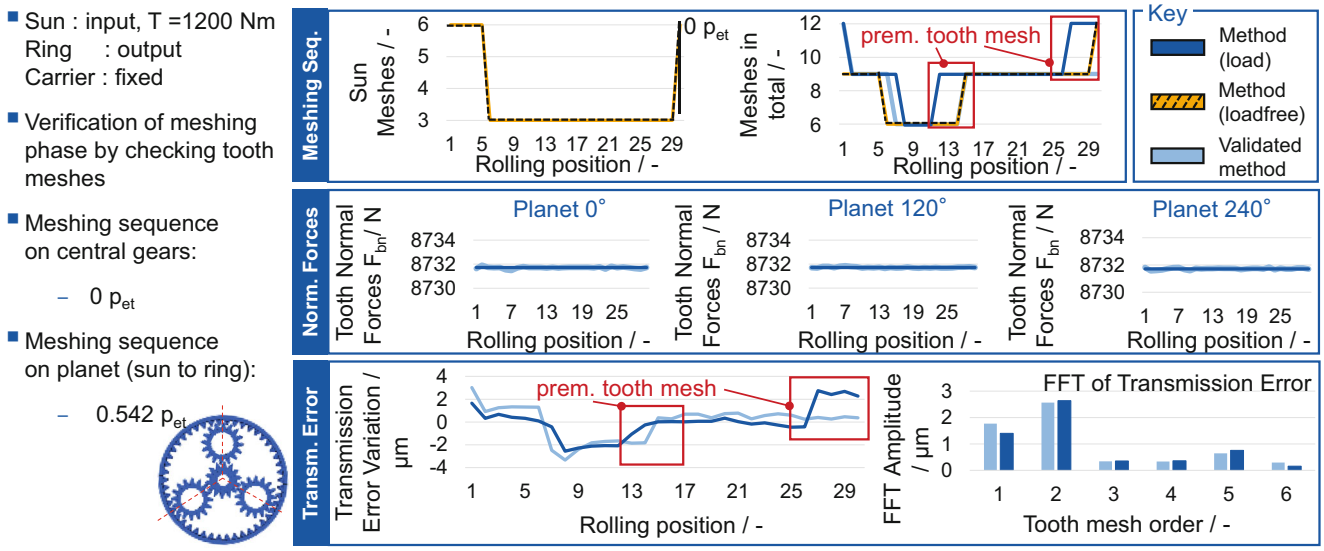

Fig. 4 Verification of the results with symmetrical meshing sequence

meshing teeth on sun gear can be verified against the pre-calculated phase position, see Fig. 5 top. The tooth meshes in total in the load-free state correspond to those of the validated method with a maximum deviation of one rolling position. The simultaneous tooth meshing of two teeth in rolling positions 5, 18 and 29 also verify the analytically determined meshing sequence at the planetary meshes by approximately one base pitch. As with the verification of the symmetrical variant, premature and late tooth meshing can be identified under load.

However, the influence of the load-related contact ratio gain is smaller than with the symmetrical variant, as the stiffness curves of the meshing areas on the central gears are out of phase. The load distribution shows very good correlation between the methods, see Fig. 5 centered. The unequal load distribution due to the phase-related meshing stiffness of the planets results in an unequal load distribution over the rolling path compared to the symmetrical variant. Differences between the tooth meshes are again shown by the premature tooth meshing of the method. In addition, in combination with the load-free meshing teeth, the phase position of the tooth meshing can be assigned to the correct planet.

Finally, TE fluctuation and amplitudes in the order spectrum of the method and the validated method show very good correlation excluding the load dependent contact ratio gain effects, see Fig. 5 below. The meshing of the planet at $\Psi = 0°$ and the planet at $\Psi = 228°$ are close to each other

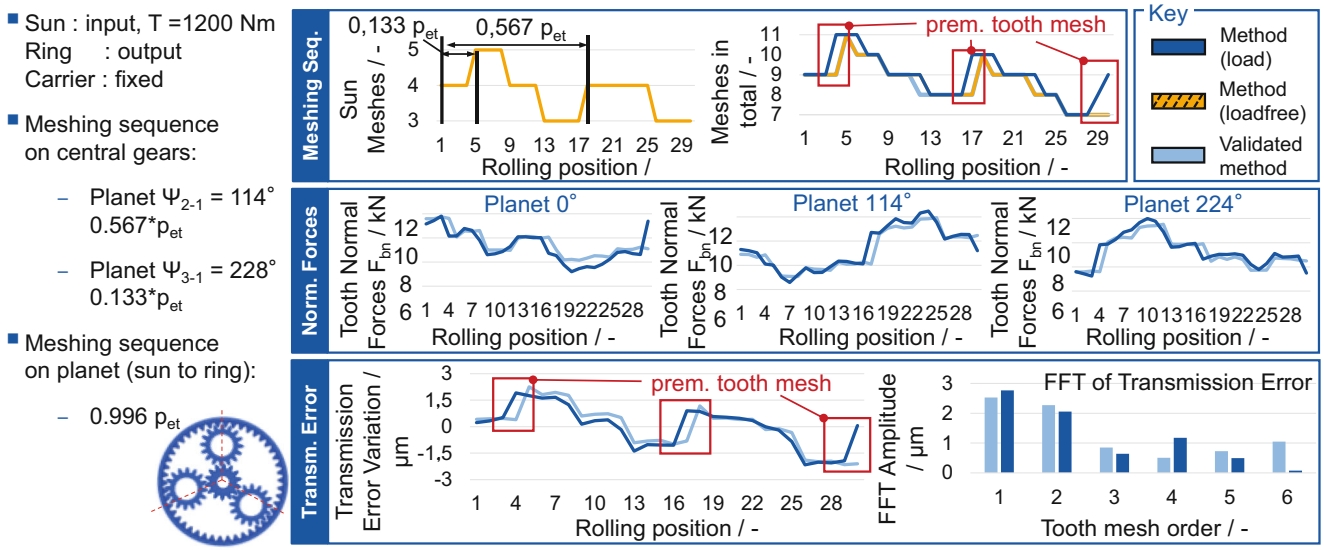

Fig. 5 Verification of unsymmetrical meshing sequence

compared to that of the planet at $\Psi = 114°$, the additional flexibility is also noticeable in the fluctuation peaks of the STE.

The method can be verified with regard to the stiffness behavior and the meshing sequences on the central gears as well as on the planet gear. It also shows that premature tooth contact under load can be identified by the newly developed method. In the future, the method can be used for micro geometry design taking into consideration load dependent contact ratio effects.

6 Quasi-static excitation behavior of long-wave deviations

Finally, a calculation study with a helical planetary gear with sequential meshing sequence on the center gears was carried out. The geometry data can be found in Table 1 on the right. The phase shift on the central gears is $\Delta_{p,Central} = 0.333 \cdot p_{et}$ on the planetary meshes with power flow from sun to ring gear $\Delta_{p,Planet} = 0.946 \cdot p_{et}$ calculated according the method by Piel [34]. Order spectra of the peak-to-peak static transmission error related to the carrier rotation were analyzed. It was evaluated in the range of the rotational orders and the first tooth mesh order $1.O_m$ as well as the peak to peak total STE variance around the mean value on the sun gear over the rotation angle. The sun was chosen as input with an input torque of $M_{IN} = 1050\,Nm$ and as output the planet carrier with fixed ring gear. Simulations were carried out without adjustable sun gear (WOAS) and with adjustable sun gear (WAS), whereby a bending stiffness $K = 479\,N/mm$ was selected in accordance to a metal bellows coupling.

Simulation results for a single planet eccentricity error of $\Delta\varepsilon = 50\,\mu m$ are shown in Fig. 6. The load distribution factor of the WOAS-variant averaged over all rolling positions is $K_\gamma = 2.5$ versus the WAS-variant with $K_\gamma = 1$ an ideal load distribution can be observed. In the order spectrum in the range of the rotational orders, the WOAS-variant excites the first planetary shaft rotation order 1st $O_{Pl} = 3.294$ and even higher harmonics. The WAS-variant shows only the 1st O_{Pl} with a lower amplitude which appears in direct proportion to the eccentricity deviation amount.

In the area of the first gear mesh order, dominant first order sidebands can be observed at a distance of 1st O_{Pl} to 1st O_m; sidebands also occur with significant amount at a distance of 3rd O_{Pl} to 1st O_m, see Fig. 6 top left. These arise as a result of the modulation effect of the tooth meshing stiffness variation by the planet rotation order. In the simulation of the WAS-variant, all order amplitudes are significantly reduced, whereby the sidebands closest to the 1st O_Z remain dominant, see Fig. 6 bottom left. This can be explained by the fact that the sidebands encounter even-numbered planetary rotational orders. Since the 1st O_{Pl} with a fixed ring gear corresponds to the ratio of the number of teeth of the ring gear and planet gear, the 1st O_t corresponds to the 17th O_{Pl} according to the number of teeth of the planet gear. The characteristic sideband orders of the WAS-variant therefore correspond to 16th O_{Pl} and 18th O_{Pl} (1st $O_m \pm$ 1st O_{Pl}) and of the WOAS-variant additionally to 14th O_{Pl} and 20th O_{Pl} (1st $O_m \pm$ 3rd O_{Pl}). This indicates a single phase sinusoidal modulation of the TE, which can be seen in particular in the TE curve of the WAS-variant, see Fig. 6 bottom right. The WOAS-variant shows an asymmetrical modulation of the TE, see Fig. 6, top right. When the planet rolling angle reaches $\varphi_{Pl} = 90°$, the eccentricity of the planet results in a pure planet position error against the direction of rotation

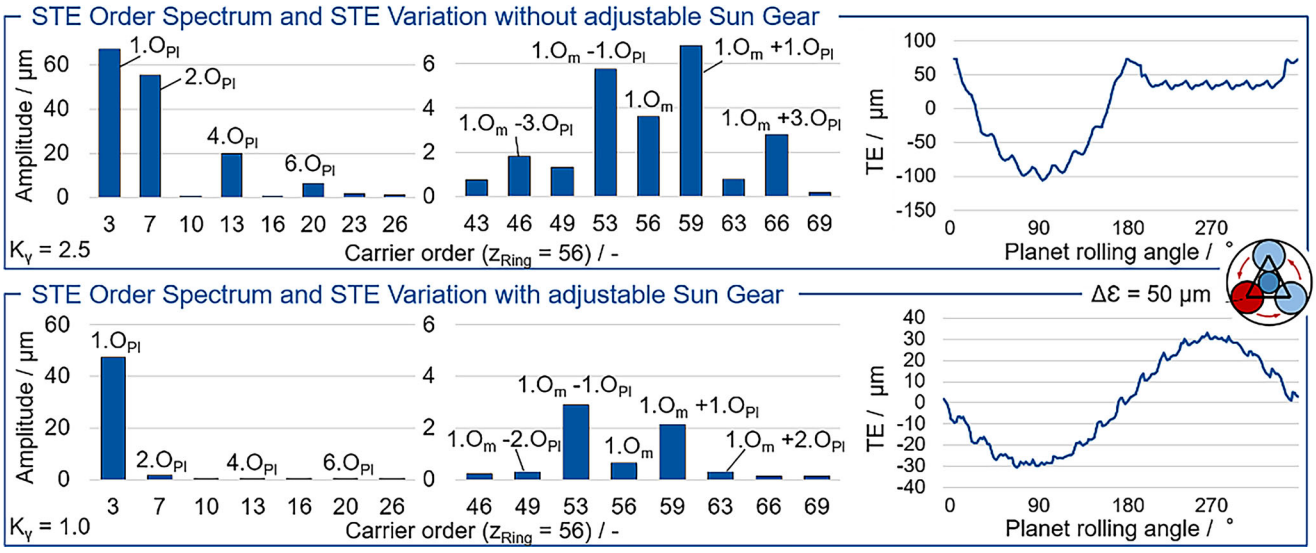

Fig. 6 Quasi-static excitation influence of planet eccentricity deviation

of the carrier, causing the single planet to take more load. At a rolling angle of $\varphi_{Pl} = 270°$, on the other hand, a planet position error results in the direction of rotation of the carrier, resulting in a load transfer to the two other planets and resulting in a lower modulation of the TE and thus higher contact stiffness. The results show the significance of an adjustable sun gear, although the 1st O_{Pl} cannot be prevented and could influence coupled planetary gear stages.

Figure 7 shows simulation results of a wobble deviation with $\Delta f\alpha = 0.03°$ of the WOAS- and WAS-variants. This corresponds to a counter-rotated eccentricity deviation of the bearing positions of the planetary shaft of $\Delta\varepsilon = 50\,\mu m$ with a distance of $L_G = 90\,mm$ to the gear center. The load distribution factor of the WOAS-variant averaged over all rolling positions is $K_\gamma = 1.2$, while the WAS-variant with $K_\gamma = 1.0$ still states an ideal load distribution between the planets. In the order spectrum in the rotational order range, see Fig. 4 left, the WOAS-variant excites the 1st O_{Pl} and 2nd O_{Pl} with similar amount as well as the planet rotation orders 3rd O_{Pl} and 4th O_{Pl}.

For the WAS-variant, the 1st O_{Pl} increases slightly, the 2nd O_{Pl} to 4th O_{Pl} decrease significantly. In the region of the first gear mesh order, see Fig. 6 center left, the sideband orders to the left of the 1st O_m of the WOAS-variant dominate and sidebands meeting both even-numbered and odd-numbered planetary rotational orders are excited. In contrast, for the WAS-variant, all sideband orders are significantly reduced, but the 1st O_m on the other hand increases almost by the factor in comparison to the WOAS-variant. The sidebands at a distance from the 2nd O_{Pl} to the 1st O_m, which meet odd-numbered O_{Pl} and arise as a result of the modulation of the meshing stiffness variation by the 1st O_{Pl}, can be observed with the highest amplitudes. The results show that the adjustable sun cannot compensate for excitation of 1st O_m and concentricity of bearing journals on the shaft has to be guaranteed.

As with the eccentricity deviation, the excited 1st O_{Pl} indicates a sinusoidal modulation of the STE, which can be seen in particular in the STE curve of the WAS-variant, see Fig. 7 bottom right. The results of the WOAS-variant show an asymmetrical modulation of the TE, see Fig. 7, top right. Depending on the helix angle direction, the chosen operating mode and the rotating direction, the wobble deviation influences the phase of the contact lines between input and output. When the planet's angle of rotation is $\varphi_{Pl} = 0°$, the planet's wobble acts as an inclination, with the planet axis on the output side facing the sun axis.

The phase shifting can be particularly observed in the STE curves at a planet rotation angle of $\varphi_{Pl} = 270°$ for both the WOAS- and WAS-variant. This angular position is a transition from a pure inclination component facing the drive side to a pure inclination against the meshing direction facing the output side. There, the contact lines of both sun and ring meshes begin with the chosen operating conditions. Regarding the WAS-variant, this effect can be reduced, but not prevented by inclination and skew of the adjustable sun, especially for the ring contact.

For planetary stages with a sequential meshing sequence, Theling was able to prove on the basis of test rig experiments that axis misalignemts of the central elements lead to a shift in the gear mesh order and higher harmonics of the STE, and establishes conditions for the occurrence of this effect [23]. A similar effect is also known in the vibration diagnosis of planetary gearboxes, where the measured acceleration amplitude by a fixed sensor is dominated by the planet rolling by close to the sensor. The tooth mesh frequency in the frequency spectrum is then modulated according to the number of planets which results to a shifting

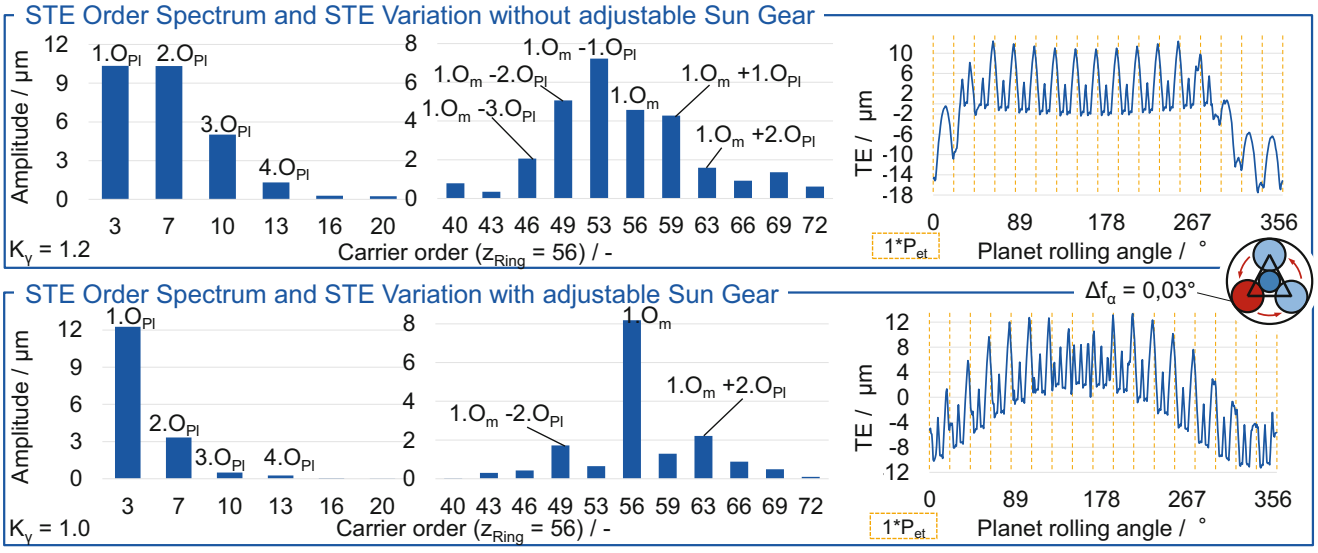

Fig. 7 Quasi-static excitation influence of a wobble deviation of one planet

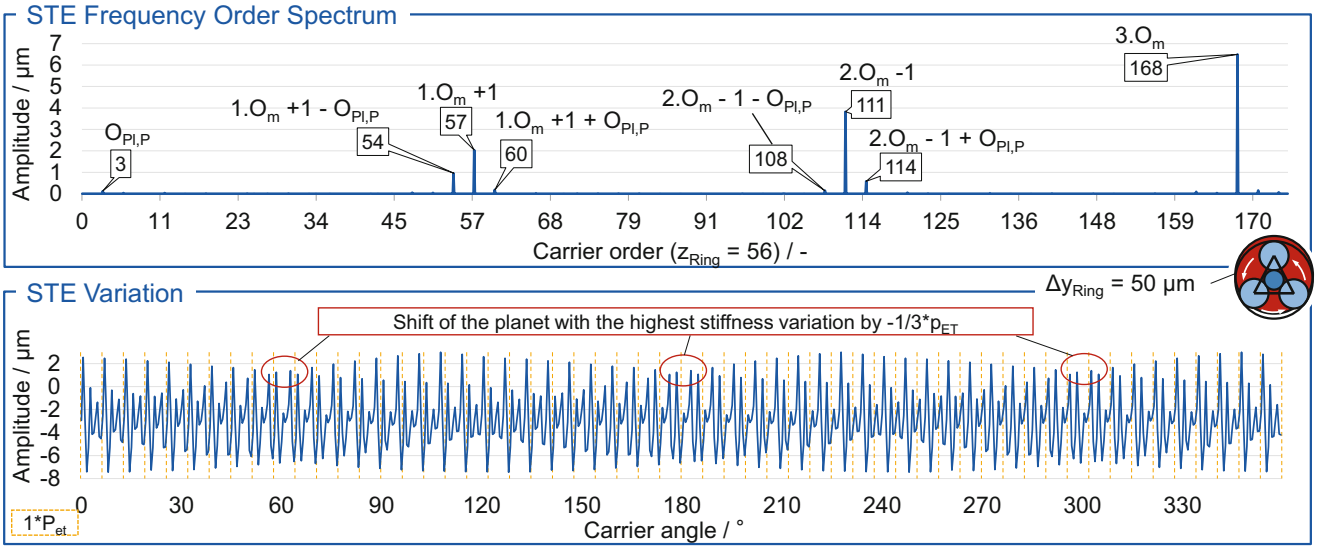

Fig. 8 Quasi-static excitation influence of fixed ring gear position deviation with adjustable sun gear

of the tooth mesh frequency in out-of-phase planetary gear configurations [8].

For this reason, an axis misalignment of the ring gear in the y-direction of $\Delta y_{Ring} = 50\,\mu m$ was simulated as a WAS-variant, see Fig. 8. The order spectrum shows that the developed method can be used to analyze the effect of the amplitude modulation of out-of-phase central gear meshes, see Fig. 8 top. Only orders that are divisible by the number of planets occur. At low amplitude, the planetary passing order $O_{Pl,P}$ can be recognized, which corresponds to the number of planets. Furthermore, the 1st O_m and 2nd O_m are each shifted to the next order that is divisible by the number of planets, while the 3rd O_m with the highest amplitude remains unshifted, as it fulfills the divisibility by the number of planets. Asymmetric sideband orders arise around the tooth mesh orders and are divisible by the number of planets.

The STE over the planet carrier rotation angle gives further information about the modulation effects, see Fig. 8 below. Essentially three envelopes can be recognized, which can be traced back to the planets with out-of-phase meshes and are offset from each other by the planet position angle. All planets pass the position, at which the ring gear axis misalignment acts as a planet position deviation in carrier rotation direction which results in a minimum of the single planet stiffness variation. The maximum on the other hand is due to the planet position where the ring gear axis misalignment acts a planet position error against the carrier rotation direction which results in a maximum of the single planet stiffness variation. Between the minimum and maximum of STE of one planet, the planet with the highest stiffness variation changes and is also in a different phase as the previous planet, see Fig. 8 below marked in red. Ultimately, the meshing stiffness oscillation of the planet shifted in phase by $-1/3 \cdot p_{et}$ increases and a phase transition takes place. As this happens three times with three planets, the meshing frequency gains an additional oscillation per carrier rotation, which visually explains the order shift of the first tooth mesh order. The phenomenon described is interesting for the application in that displacements of the central elements due to manufacturing, assembly and weight influences as well as non-torque loads can rarely be prevented. Deviations of central elements, including those from the planet carrier, should be analyzed for specific applications in the future. The method proves to consider modulation phenomena taking into consideration load dependent effects and is also able to evaluate flank pressure and tooth root stress based on the determined contact forces which are to be evaluated in the future.

7 Summary and outlook

An FE-based method with surface contact and numerical line contact was developed, which considers coupled planetary gear meshing taking into account long-wave axis misalignments in a quasi-static tooth contact analysis. In addition, an algorithm was implemented considering compensation of uneven load-sharing by an adjustable sun gear arrangement. The Method solves FE-Stiffnesses independent from contact lines with a general FE-Solver. Further an iterative contact finding is performed between the tooth flank notes to establish the meshing phases between the Planets on the central gears as well as between the contact on each planet. Further the method interpolates the meshing areas to a numerical line contact considering pre-

mature tooth meshing under load. For the load calculation the nodal FE-Stiffness and contact distances are transferred into a linear spring equation system. An iterative load calculation and contact finding approach was implemented to consider radial and angular sun displacement and simulate the load sharing behavior, additional static transmission error as well as the sun trajectory itself dependent on a given sun connection stiffness.

The method is verified against a validated method with an analytical line contact approach. The results show very good correlation, whereby the new method can consider premature tooth contact under load. Furthermore, deviations with long-wave excitation behavior with rotating carrier with and without adjustable sun gear were investigated. The presented results shows relevance of adjustable central elements in practice of planetary gears.

The results with regard to the eccentricity and comparable wobble deviation of a planetary gear indicate a higher influence of the wobble deviation on the excitation behavior compared to the eccentricity deviation for the analyzed gear set and configuration. Additionally, there is a lacking ability of the adjustable sun gear to compensate excitation of the first gear mesh order by the wobble deviation. Furthermore, sidebands can be identified and traced back to the planet rotation orders. When investigating simulation results of eccentricities, it can be observed that only even-numbered planet rotation orders and sideband orders that fall on these are excited by a significant amplitude. Static axis misalignments of the central elements have a long-wave excitation influence with a rotating planet carrier. This can also be observed on a simulation result using the method for a ring gear position error. The shifting of the gear mesh order is reasonable and consistent with investigations in the state of the art [23].

The validation of the method on a planetary gear test rig using STE signal curves and specifically manufactured axis misalignments is the next step. Furthermore, the influence of the stiffness of the planet carrier on the planetary gears analog to the method for calculating the adjustable sun gear should be implemented into the method to determine the cross influence between deviated meshing condition and surrounding stiffness. For the signal analysis method based on a fixed sensor position, the transfer path must be modeled. Subsequently, based on speed and torque data as well as the modeling of planetary stages in the tooth contact analysis, estimated signals can be simulated at a fixed sensor position. The reverse path can then be analyzed to infer the displaced tooth contact based on the operating data and to deduce the remaining service life of the planetary gearbox from a local stress calculation in combination with historical data. In addition to the operating data, displacement data of the sun shaft could be included in order to increase the correlation quality between displacements occurring during operation and those determined by simulation.

Acknowledgements The authors gratefully acknowledge the Federal Ministry for Economic Affairs and Climate Action for providing the financial support for the Project [IGF 22631 N] based on a resolution of the German Parliament.

Federal Ministry
for Economic Affairs
and Climate Action

Funding Open Access funding enabled and organized by Projekt DEAL.

Statement and Declarations

Conflict of interest S. Nohl, C. Westphal and C. Brecher declare that they have no competing interests.

References

1. Dao C, Kazemtabrizi B, Crabtree C (2019) Wind turbine reliability data review and impacts on levelised cost of energy. Wind Energ 22(12):1848–1871. https://doi.org/10.1002/we.2404
2. Hau E (2016) Windkraftanlagen. Grundlagen, technik, einsatz, wirtschaftlichkeit, 6th edn. Springer Vieweg, Berlin
3. Theling J, Löpenhaus C, Brecher C (2019) Influence of planet carrier misalignments on the operational behavior of planetary gearboxes. In: WZL Getriebekreis (Hrsg) gear and transmission research, vol 14-1. Apprimus Verlag, Aachen, pp 14–22
4. Muuß T (2005) Condition monitoring systeme für windenergieanlagen einsatz und zertifizierung. Dtsch. Ges. Zerstörungsfreie Prüf 94-CD(27):1–10
5. Collacott RA (1977) Mechanical fault diagnosis and condition monitoring. Chapman and Hall; Wiley; Distributed in the U.S.A. by Halsted Press, London, New York
6. Scheffer C, Girdhar P (2004) Practical machinery vibration analysis and predictive maintenance. Practical professional books from Elsevier. Elsevier, Amsterdam, Boston
7. Theling J, Brimmers J, Brecher C (2022) Influences on the excitation behavior of lightweight planetary gearboxes. Forsch Ingenieurwes 86(3):303–313. https://doi.org/10.1007/s10010-021-00512-8

8. Inalpolat M, Kahraman A (2009) A theoretical and experimental investigation of modulation sidebands of planetary gear sets. J Sound Vib 323(3–5):677–696. https://doi.org/10.1016/j.jsv.2009.01.004
9. Götz JG (2023) Anregungs- und Schwingungsverhalten von Planetengetrieben. Diss. Technische Universität München
10. Zhang K, Li H, Cao S, Wang C, Sun B, Liu A (2022) Investigation on planetary gearbox fault mechanism under variable speed conditions based on rigid-flexible coupling dynamics model. Eng Fail Anal 133:105994. https://doi.org/10.1016/j.engfailanal.2021.105994
11. Feng Z, Zuo MJ (2012) Vibration signal models for fault diagnosis of planetary gearboxes. J Sound Vib 331(22):4919–4939. https://doi.org/10.1016/j.jsv.2012.05.039
12. Inalpolat M, Kahraman A (2010) A dynamic model to predict modulation sidebands of a planetary gear set having manufacturing errors. J Sound Vib 329(4):371–393. https://doi.org/10.1016/j.jsv.2009.09.022
13. Xie C, Yu W (2022) Gear dynamic modelling based on the concept of dynamic mesh stiffness: theoretical study and experimental verification. J Mech Sci Technol 36(10):4953–4965. https://doi.org/10.1007/s12206-022-0909-9
14. Westphal C, Brimmers J, Brecher C (2023) Influence of axis misalignments in stepped planetary gear stages on the excitation behavior—test rig development and simulative analysis. Forsch Ingenieurwes 87(3):1103–1116. https://doi.org/10.1007/s10010-023-00709-z
15. Thoret-Bauchet Q, Velex P, Guingand M, Casanova P (2019) Simulations of the dynamic response of planetary gears in the presence of localised tooth faults. Proc Inst Mech Eng Part C: J Mech Eng Sci 233(21–22):7212–7223. https://doi.org/10.1177/0954406219846153
16. Shen J, Hu N, Zhang L, Luo P (2020) Dynamic analysis of planetary gear with root crack in sun gear based on improved time-varying mesh stiffness. Appl Sci 10(23):8379. https://doi.org/10.3390/app10238379
17. Luo W, Qiao B, Shen Z, Yang Z, Cao H, Chen X (2021) Investigation on the influence of spalling defects on the dynamic performance of planetary gear sets with sliding friction. Tribol Int 154:106639. https://doi.org/10.1016/j.triboint.2020.106639
18. Bejar F, Perret-Liaudet J, Bareille O, Ichchou M, Fontana M (2024) Review and benchmarking study of different gear contact analysis software in terms of the static transmission error response. Results Eng 22:102286. https://doi.org/10.1016/j.rineng.2024.102286
19. Schäfer J (2008) Erweiterung des Linienkontaktmodells für die Finite-Elemente-basierte Zahnkontaktanalyse von Stirnradverzahnungen. Diss. RWTH Aachen University
20. Neupert B (1983) Berechnung der Zahnkräfte Pressungen und Spannungen von Stirn- und Kegelradgetrieben. Diss. RWTH Aachen University
21. Weck M, Schlattmeier H, Schäfer J (eds) (2003) Kontaktmodell mehrfacher Zahneingriff. Berechnung von Stirnradpaarungen mit Mehrfacheingriffen mit Hilfe der Finite-Elemente-Methode, Frankfurt a. M.
22. Ingeli J (2018) Erweiterung der FE-basierten zahnkontaktanalyse zur normkonformen Grübchentragfähigkeitsberechnung symmetrischer und asymmetrischer Verzahnungen. Diss. RWTH Aachen University
23. Theling J (2023) Auslegung von Planetengetrieben im elastischen Verzahnungsumfeld unter Berücksichtigung der Wechselwirkungen des Mehrfacheingriffes. Diss. RWTH Aachen
24. Wittke W (1994) Beanspruchungsgerechte und geräuschoptimierte Strinradgetriebe Toleranzvorgaben und Flankenkorrekturen. Diss. RWTH Aachen University
25. Ahmad M (2023) Anregungsgerechte Auslegung und Tolerierung schnelllaufender Getriebe unter Berücksichtigung kurz- und langwelliger Verzahnungsabweichungen. Diss. RWTH Aachen University
26. Hemmelmann JE (2007) Simulation des lastfreien und belasteten Zahneingriffs zur Analyse der Drehübertragung von Zahnradgetrieben. Diss. RWTH Aachen University
27. Brecher C, Brimmers J, Westphal C (2019) Einfluss der dynamischen Lastverteilung in Zahnkontakten auf das Systemverhalten. In: Dr.-Ing. Schlecht B (ed) Dresdner Maschinenelemente Kolloquium DMK 2019, pp 353–372
28. Neubauer B (2016) Lastverteilung und Anregungsverhalten in Planetengetriebensystemen. Bestimmung des Lastaufteilungsverhaltens, Berechnung und Optimierung der Lastverteilung und des Anregungsverhaltens. TU München (in den Zahneingriffen von Planetengetrieben in Wechselwirkung mit dem komplexen Getriebeumfeld. Diss)
29. Heider MK (2012) Schwingungsverhalten von Zahnradgetrieben. Beurteilung und Optimierung des Schwingungsverhaltens von Stirnrad- und Planetengetrieben. Zugl.: München, Techn. Univ., Diss, 1st edn. Dissertationen der FZG / Forschungsstelle für Zahnräder und Getriebebau, Technische Universität München, Bd 185. Verl. Dr. Hut, München
30. Willecke M, Brimmers J, Brecher C (2023) Surrogate model based prediction of transmission error characteristics based on generalized topography deviations. Forsch Ingenieurwes 87(1):431–440. https://doi.org/10.1007/s10010-023-00647-w
31. Bastert C-C (1971) Die Verlagerung der Zentralräder in Planetengetrieben. Forsch Ingenieurwes 37(1):21–29. https://doi.org/10.1007/BF02560480
32. Westphal C, Brimmers J, Brecher C (2020) Analysis of the operational behavior of a high-speed planetary gear stage for electric heavy-duty trucks in multi-body simulation. In: AGMA, American Gear Manufacturers Association (Hrsg) (ed) AGMA fall technical meeting
33. Papies J (2014) Methodik zur systematischen Analyse und Optimierung dynamischer Kraft- u. Weganregungen in Planetengetrieben. Diss. Ruhr-Universität Bochum
34. Piel D (2020) Methode zur Beschreibung und Optimierung des Anregungsverhaltens von Planetengetrieben. Diss. RWTH Aachen University